

1 **Title:** The interaction of shockwaves with a vapour bubble in boiling histotripsy: The shock
2 scattering effect.

3 **Author names and affiliations:** Ki Joo Pahk¹, Sunho Lee², Pierre G lat³, Matheus Oliveira de
4 Andrade³ and Nader Saffari³

5 ¹Center for Bionics, Biomedical Research Institute, Korea Institute of Science and Technology
6 (KIST), Seoul, 02792, Republic of Korea

7 ²Department of Bio and Brain Engineering, Korea Advanced Institute of Science and
8 Technology, Daejeon, 34141, Republic of Korea

9 ³Department of Mechanical Engineering, University College London, London, WC1E 7JE, UK

10

11 **Corresponding author:**

12 Ki Joo Pahk

13 Center for Bionics, Biomedical Research Institute, Korea Institute of Science and Technology
14 (KIST), Seoul, 02792, Republic of Korea

15 E-mail: kjpahk@kist.re.kr

16

17

18

19

20

21

22

23

24

25

1 **Abstract**

2 Boiling histotripsy is a High Intensity Focused Ultrasound (HIFU) technique which uses a
3 number of short pulses with high acoustic pressures at the HIFU focus to induce mechanical
4 tissue fractionation. In boiling histotripsy, two different types of acoustic cavitation contribute
5 towards mechanical tissue destruction: a boiling vapour bubble and cavitation clouds. An
6 understanding of the mechanisms underpinning these phenomena and their dynamics is
7 therefore paramount to predicting and controlling the overall size of a lesion produced for a
8 given boiling histotripsy exposure condition. A number of studies have shown the effects of
9 shockwave heating in generating a boiling bubble at the HIFU focus and have studied its
10 dynamics under boiling histotripsy insonation. However, not much is known about the
11 subsequent production of cavitation clouds that form between the HIFU transducer and the
12 boiling bubble. The main objective of the present study is to examine what causes this bubble
13 cluster formation after the generation of a boiling vapour bubble. A numerical simulation of
14 2D nonlinear wave propagation with the presence of a bubble at the focus of a HIFU field was
15 performed using the k-Wave MATLAB toolbox for time domain ultrasound simulations, which
16 numerically solves the generalised Westervelt equation. The numerical results clearly
17 demonstrate the appearance of the constructive interference of a backscattered shockwave by
18 a bubble with incoming incident shockwaves. This interaction (i.e., the reflected and inverted
19 peak positive phase from the bubble with the incoming incident rarefactional phase) can
20 eventually induce a greater peak negative pressure field compared to that without the bubble at
21 the HIFU focus. In addition, the backscattered peak negative pressure magnitude gradually
22 increased from 17.4 MPa to 31.6 MPa when increasing the bubble size from 0.2 mm to 1.5 mm.
23 The latter value is above the intrinsic cavitation threshold of -28 MPa in soft tissue. Our results
24 suggest that the formation of a cavitation cloud in boiling histotripsy is a threshold effect which
25 primarily depends (a) the size and location of a boiling bubble, and (b) the sum of the incident
26 field and that scattered by a bubble.

27

28 **Keywords:** high intensity focused ultrasound; acoustic cavitation; boiling histotripsy; a boiling
29 bubble; cavitation clouds; shock scattering.

30

31

32

1. Introduction

Boiling histotripsy is a High Intensity Focused Ultrasound (HIFU) technique that employs a number of millisecond long HIFU pulses with high peak positive P_+ and negative P_- pressures at the HIFU focus ($P_+ > 40$ MPa and $P_- < 10 - 15$ MPa). This results in mechanical tissue fractionation without causing any significant thermal damage. Acoustic cavitation generated during boiling histotripsy exposure is the main mechanism for tissue fractionation [1-3]. A number of *ex-* and *in vivo* boiling histotripsy studies have clearly demonstrated that a well-defined lesion that contains complete fragmentation of soft tissue or acellular debris can be produced in the kidney, liver, heart and cardiac muscle [2-7].

10

Contrary to a symmetric “cigar”-shaped thermally ablated lesion induced by traditional HIFU thermal ablation, boiling histotripsy produces a tadpole shaped lesion, consisting of a head and a tail with the head located towards the HIFU transducer [8]. The principle mechanisms behind this particular lesion shape formation, as opposed to a “cigar” shape, are thought to be due to the presence of boiling vapour bubbles and of inertial cavitation clouds during boiling histotripsy exposure [9]. Mechanisms of boiling histotripsy have been extensively investigated over the past 10 years. Nonlinear shocked waves with high acoustic pressure amplitudes induced at the HIFU focus in soft tissue can increase tissue temperature to boiling in a few milliseconds via shock wave heating effect [1, 2]. The interaction of this localised tissue heating with the incoming acoustic waves can then lead to the generation of a boiling vapour bubble at the HIFU focus [10], which expands to around a millimetre in size through rectified growth behaviour [11]. This growth is thought to be due to the combination of the asymmetry in a nonlinear shocked wave and water vapour that transports into the bubble [12, 13]. The extent of this growing bubble at the HIFU focus is, however, likely to be limited to the localised shockwave heated zone because of the large temperature gradient across the edge of the heated

1 region [13]. Further interaction of this enlarged boiling bubble with incoming incident
2 shockwaves can then induce inertial cavitation clouds that form in front of the boiling bubble,
3 progressing towards the HIFU source until it is switched off [9]. The shear stresses produced
4 around an oscillating boiling bubble and emissions of micro jetting and shockwaves resulting
5 from violent bubble collapses involved in inertial cavitation clouds can tear off soft tissue [2,
6 11]. This leads to the formations of the tail and subsequently the head of a boiling histotripsy
7 lesion (see Figure 1). Because these two different types of bubble activity appear during boiling
8 histotripsy exposure (boiling bubble and cavitation clouds), the nature of the resulting
9 mechanical damage in cellular structures around the tail and the head of the lesion are also
10 distinct from one another. For instance, it has been reported that the margins of the tail of a
11 boiling histotripsy lesion produced in liver *in vivo* are sharply demarcated with smooth
12 boundaries whereas broken hepatocyte plates with ragged boundaries are observed around the
13 head of a boiling histotripsy lesion [11].

14
15 Whilst a number of studies have shown the effects of shockwave heating in creating a boiling
16 bubble at the HIFU focus and have studied its rectified growth behaviour in soft tissue during
17 the course of boiling histotripsy exposure [1, 2, 9, 11-13], little is known about the subsequent
18 formation of cavitation clouds. In fact, it is of paramount importance to understand the
19 generation of this bubble cluster in order to predict as well as to control the overall size of a
20 lesion induced under a given boiling histotripsy exposure condition. In our previous study [9],
21 we hypothesised that (a) the interaction of incoming incident shockwaves with a boiling vapour
22 bubble would lead to the formation of cavitation clouds and (b) the extent of the head of a
23 boiling histotripsy lesion would be primarily dependent upon the pressure magnitude of a
24 backscattered acoustic field by a bubble. To support our hypothesis, the present study aims to
25 investigate what causes the subsequent bubble cluster formation in boiling histotripsy. A

1 numerical simulation of nonlinear wave propagation with the presence of a scatterer (i.e. a
 2 bubble) at the HIFU focus in a heterogeneous medium is performed. A qualitative analysis is
 3 conducted in order to capture basic features of the interactions of a shockwave with a bubble.

4

5 **2. Numerical methods**

6 High speed camera experimental results of bubble dynamics induced in a liver tissue phantom
 7 were reported in our previous boiling histotripsy studies [9, 11]. These results clearly showed
 8 the subsequent formation of a cavitation cloud in front of a primary boiling vapour bubble at
 9 the HIFU focus, resulting in the production of the head of a boiling histotripsy lesion. To gain
 10 further insight into the mechanisms behind the observed phenomena, a numerical study of the
 11 interaction of a shockwave with a vapour bubble immersed in a liver tissue phantom was
 12 carried out. The simulations were conducted using the open source k-Wave v1.2 MATLAB
 13 toolbox. k-Wave numerically solves the generalised Westervelt equation which accounts for
 14 heterogeneities in the ambient mass density, material nonlinearity (second-order nonlinearity),
 15 and power law absorption and dispersion [14-16]. The experimental validation of k-Wave has
 16 been performed for nonlinear wave propagation in a homogenous medium [17] as well as in a
 17 heterogeneous medium with simple geometric scatterers such as rectangular and wedge shaped
 18 olive oils or glycerol filled phantoms [18, 19]. The generalised Westervelt equation describing
 19 nonlinear wave propagation in heterogeneous media has the following form [20]

$$20 \quad \nabla^2 p_a - \frac{1}{c_0^2} \frac{\partial^2 p_a}{\partial t^2} - \frac{1}{\rho_0} \nabla \rho_0 \cdot \nabla p_a + \frac{\beta}{\rho_0 c_0^4} \frac{\partial^2 p_a^2}{\partial t^2} + \left(\tau \frac{\partial}{\partial t} (-\nabla^2)^{y/2} + \eta (-\nabla^2)^{(y+2)/2} \right) p_a = 0 \quad (1)$$

21 where p_a is the acoustic pressure, c_0 is the speed of sound in the medium, ρ_0 is the density of the
 22 medium, t is time, $\beta = (1 + B/2A)$ is the coefficient of nonlinearity and B/A is the nonlinear
 23 parameter of the medium. A and B are the coefficients of the first and second order terms of
 24 the Taylor series expansion of the pressure-density relation. τ and η are respectively the

1 absorption and dispersion proportionality coefficients. γ is the material dependent power law
2 exponent. To solve the governing partial differential equation (1), k-Wave uses the k -space
3 pseudospectral method [21] where the Fourier collocation spectral method is used to compute
4 spatial gradients. Compared to other available finite difference and finite element methods, the
5 k -space pseudospectral method theoretically allows for much coarser grid spacings and larger
6 time steps for the same degree of accuracy [17]. A detailed description of the k-Wave toolbox
7 can be found in [16].

8
9 Simulating 3D nonlinear wave propagation in heterogeneous media is costly in terms of both
10 memory consumption and computational time. For instance, the numerical 3D simulation of 1
11 MHz nonlinear wave propagation up to the 40th harmonic (i.e., 40 MHz) requires at least $2^{12} \times$
12 $2^{12} \times 2^{12}$ grid points (total of 6.872×10^{10} points) with a computational domain size of 75×75
13 $\times 75$ mm, using a discretisation of two points per wavelength (PPW). Moreover, significant
14 wave distortion in soft tissue can lead to the formation of a shock wavefront at the HIFU focus
15 which contains tens of higher multiple harmonics of the fundamental frequency [1]. A larger
16 number of PPW is, therefore, needed to resolve a steep shock wave front where the pressure
17 drastically increases over a very short time (i.e. of order of nanoseconds) [22]. In addition, the
18 Courant-Friedrichs-Lewy number ($CFL \equiv c_0 \Delta t / \Delta x$), which is defined as the ratio of the distance
19 a wave can travel in one time step Δt to the grid spacing Δx [17], also needs to be small enough
20 to achieve sufficient accuracy (i.e., $CFL \leq c_0 / c_{\max}$ where c_{\max} is the maximum speed of sound
21 in the medium). All the aforementioned factors will eventually increase computational
22 overheads in terms of run times and memory consumption. To reduce computational time while
23 achieving sufficient accuracy and capturing basic features of the interaction of a nonlinear wave
24 with a bubble, in the present study, we performed 2D simulation of nonlinear wave propagation
25 in a heterogeneous medium. For simplicity, a vapour bubble at the HIFU focus was modelled

1 as a stationary 2D infinite cylinder whose acoustic properties are equal to those of water vapour.
2 Furthermore, the effects of acoustic emissions resulting from bubble oscillations under HIFU
3 exposure on wave propagation were also not accounted for in the simulations.

4
5 A schematic diagram illustrating the geometrical model used in the simulations performed is
6 shown in Figure 2. A 1.0 MHz single element bowl-shaped HIFU transducer with an aperture
7 size of 64 mm and a radius of curvature of 62.6 mm was considered. This modelled HIFU
8 source has the same geometry as the H-series HIFU transducers from Sonic Concepts (Bothell,
9 WA, USA). The H-series transducers have been widely used in boiling histotripsy experiments
10 [2, 6, 9, 11, 13]. In the simulations, 1 MHz HIFU waves propagated through a layer of water
11 followed by a liver tissue phantom layer. A scatterer in the form of a vapour bubble was located
12 4.7 mm beyond the water-liver tissue phantom interface at the HIFU focus (i.e. at 62.3 mm in
13 the axial direction), as shown in Figure 2. The total grid size used was $2^{13} \times 2^{13}$ points with a
14 computational domain size of 75.51×75.51 mm including a perfectly matched layer (PML) of
15 20×20 grid points on each side of the domain. 160 PPW (nonlinear propagation up to the 67th
16 harmonic of the fundamental frequency, see the convergence test shown in Figures 4 and 5)
17 and a CFL number of 0.05 with a temporal step size Δt of 0.3 ns and a grid spacing (Δx and
18 Δy) of 9.26 μm in the axial and lateral directions were used in the simulation. The physical
19 properties used in the simulations are listed in Table 1. All simulations were performed on a
20 desktop PC with 3.6 GHz CPU (i7-9700K), 16 GB of RAM and NVIDIA GeForce RTX 2080
21 Ti (11 GB) GPU. Each simulation took around 13 hours to complete. Figure 3 depicts an
22 example showing simulated acoustic fields with and without the presence of a bubble under
23 linear propagation conditions using k-Wave as implemented in the present study. The axial and
24 lateral full width half maxima of the pressure field of the HIFU source were, respectively, 12.27
25 mm and 1.72 mm.

1 Lastly, the pressure amplitude of an input sinusoidal signal used in the simulations gradually
2 increased until a well-defined nonlinear shocked wave with $P_+ \geq 40$ MPa and $P_- \leq 8 - 15$ MPa
3 appeared in the absence of a bubble at the HIFU focus. In this work, a shock wave is defined
4 as a strongly distorted nonlinear wave with a very rapid rise time (< 50 ns), $P_+ \geq 35$ MPa and
5 P_- of about 10 MPa [23].

6
7 To investigate the interaction of incident shockwaves with a bubble, it is crucially important to
8 accurately model the formation of a shock wave front at the HIFU focus that contains tens of
9 higher harmonics of the fundamental frequency. In addition, because of the large acoustic
10 impedance mismatch at the liver tissue phantom-bubble interface, most of the higher frequency
11 components would likely be reflected back to the HIFU source from the bubble, generating the
12 backscattered acoustic field. In this study, a 1D convergence test was, therefore, carried to
13 examine how well k-Wave could model 1 MHz nonlinear wave propagation with 160 PPW
14 and a CFL number of 0.05. To do this, one of k-Wave's given examples,
15 *example_na_modelling_nonlinearity.m*, which describes the characteristics of the nonlinearity
16 encapsulated by the first-order k-Wave simulation functions, was employed to simulate the
17 propagation of plane progressive waves in the liver tissue phantom. In this test set-up, an input
18 source pressure gradually increased until the shape of the time domain wave signal changed
19 from a sine wave to an 'N'-like wave. These 1D simulations results were then compared with
20 the series solution given by Mendousse [29], which are shown in Figure 4. In all cases, there
21 is a good agreement between the theoretical and numerical results with a maximum error of
22 0.09% appearing at the fundamental frequency (1 MHz). With 160 PPW, the maximum
23 supported frequency in k-Wave is 80 MHz (two points per wavelength at the highest generated
24 harmonic). However, at this grid density, k-Wave appeared unable to resolve the harmonic
25 content beyond the 67th harmonic (67 MHz) (Figure 4d-ii), relative to the Mendousse solution.

1 Our numerical analysis of the interaction of 1 MHz nonlinear wave with a bubble is, therefore,
2 likely to be limited to a maximum frequency of 67 MHz. This particularly applies to the
3 backscattered field by a bubble.

5 **3. Results**

6 In the present study, a numerical simulation was performed to investigate the interaction of
7 shockwaves with a bubble at the HIFU focus in a viscoelastic medium (i.e., liver tissue
8 phantom) during the course of boiling histotripsy exposure. For simplicity and to capture the
9 essential feature of the interaction of a shockwave and a bubble, a bubble was modelled as a
10 non-translational 2D infinite cylinder whose properties are equal to those of water vapour. This
11 2D cylinder is hereafter referred to as a bubble. Figure 6 shows simulated 2D spatial
12 distributions of nonlinear acoustic fields and 1D nonlinear waveforms at a given distance in
13 the HIFU axial direction in the absence of a bubble at the HIFU focus. A shockwave with P_+
14 of 51.2 MPa and P_- of -9.8 MPa can be obtained from the k-Wave simulations (Figure 6e). In
15 contrast with the linear propagation conditions (Figures 3a and b), the computed positive and
16 negative pressure fields are no longer the same (Figures 6a and b). This is because of the
17 distortion of an initially harmonic acoustic waveform due to tissue nonlinearity, which leads to
18 the asymmetry in the compressional and rarefactional pressure phases. As can be observed in
19 Figure 6e, the asymmetry is greatest at the HIFU focus where nonlinear effects are the strongest
20 [1].

21
22 After the confirmation of the presence of a shockwave at the HIFU focus in the absence of a
23 bubble, nonlinear acoustic fields scattered by a bubble were then computed with the same set
24 of input parameters which were used to obtain Figure 6 (i.e., P_+ of 51.2 and P_- of -9.8 MPa).

1 Since the acoustic cavitation threshold is primarily dependent on the peak negative pressure at
 2 a given driving frequency [12], the changes in the magnitude of negative pressure fields as a
 3 function of changes in the bubble size were analysed. The diameter of the bubble was varied
 4 from 154 μm ($1/10^{\text{th}}$ of the wavelength λ at 1 MHz) to 1.544 mm (equal to λ). Figure 7 shows
 5 the simulated 1 MHz nonlinear acoustic fields around a 154 μm -sized bubble. Interestingly,
 6 strong negative pressure fields between the HIFU transducer and the bubble are clearly
 7 observed with (a) the peak negative pressure of $P_- = -17.4$ MPa (Figure 7d) and (b) the
 8 presence of the constructive interference of the backscattered shockwave by the bubble with
 9 the incoming incident shockwaves (indicated by the red arrows in Figures 7c to e). The highest
 10 negative pressure magnitude appears at 61.56 mm along the axial direction, in front of the
 11 bubble, and the backscattered pressure amplitudes gradually decrease towards the HIFU
 12 transducer. Furthermore, the peak negative pressure P_- rises from -17.4 to -31.6 MPa as the
 13 bubble size increases or becomes close to the wavelength of 1.544 mm (Figure 8). Partially
 14 shielded acoustic pressure fields are observed behind a bubble in all the simulation cases
 15 (Figures 7a and b, and Figures 8a-i,-ii, b-i, -ii, and c-i, -ii).

16

17 An additional calculation was performed in order to investigate the effects of the changes in
 18 the peak positive and negative pressure amplitudes of incident shockwaves ($P_{+, \text{incident}}$ and $P_{-, \text{incident}}$)
 19 on the peak negative pressure magnitude of the acoustic fields backscattered by a bubble
 20 ($P_{-, \text{backscatter}}$). A bubble with a diameter of 515 μm ($1/3^{\text{rd}}$ of the wavelength) was exposed to 1.0
 21 MHz nonlinear shocked waves under four different exposure conditions: (1) $P_{+, \text{incident}}$ of 19.5;
 22 $P_{-, \text{incident}}$ of -6.9 MPa, (2) $P_{+, \text{incident}}$ of 28.3; $P_{-, \text{incident}}$ of -7.8 MPa, (3) $P_{+, \text{incident}}$ of 43.3; $P_{-, \text{incident}}$
 23 of -9.0 MPa, and (4) $P_{+, \text{incident}}$ of 51.2, $P_{-, \text{incident}}$ of -9.8 MPa at the HIFU focus in the
 24 absence of a bubble. Figure 9 depicts the simulated acoustic fields around the bubble at a given
 25 $P_{+, \text{incident}}$ and $P_{-, \text{incident}}$. Overall, the peak negative pressure field generated between the HIFU

1 source and the bubble increases with increasing pressure amplitudes of the incident
2 shockwaves. Furthermore, it can be observed that the $P_{+, \text{incident}}$ has a great impact on the $P_{-, \text{backscatter}}$. The peak negative pressure of the backscattered acoustic field by the bubble under $P_{+, \text{incident}} = 51.2$ and $P_{-, \text{incident}} = -9.8$ MPa is, for instance, 5 MPa greater than that obtained with $P_{+, \text{incident}} = 43.3$ and $P_{-, \text{incident}} = -9.0$ MPa (Figures 9b and c, Table 2). In this comparison, the differences in $P_{+, \text{incident}}$ and $P_{-, \text{incident}}$ are 7.9 and 0.8 MPa, respectively. This is summarised in Table 2.

8
9 Figure 10 shows the effects of the changes in the location of a bubble on backscattered acoustic fields in boiling histotripsy. In the simulations, the size of a bubble (i.e., 515 μm) as well as the exposure condition ($P_{+, \text{incident}}$ of 51.2, $P_{-, \text{incident}}$ of -9.8 MPa) were kept constant, whilst the position of the bubble was varied as 58.3, 60.3, 64.3 or 66.3 mm along the HIFU axial axis. Both the peak positive and negative pressure magnitudes of the acoustic fields scattered by the bubble gradually increase as the bubble moves towards the HIFU focus.

16 **4. Discussions**

17 Boiling histotripsy is a promising HIFU technique which can be used to mechanically fractionate solid tumours. Mechanical damage in the shape of a tadpole (i.e., a head and a tail) is typically observed at the HIFU focus following boiling histotripsy treatment (Figure 1) [6, 8, 9]. A number of *ex-* and *in vivo* studies have clearly shown the effects of boiling histotripsy in removing target tissue at the HIFU focus. However, studies of the control and prediction of the shape and size of a boiling histotripsy lesion for pre-treatment planning have not yet been performed. This is likely to be due to a limited understanding of the mechanisms underpinning the lesion generation during boiling histotripsy exposure, particularly the formation of the head.

1 Our previous works [9, 11] have clearly demonstrated that the tail of a boiling histotripsy lesion
2 is formed by shear stresses induced around an oscillating boiling bubble within a localised
3 heated region, whereas the subsequent formation of cavitation clouds and their violent
4 collapses are likely to be responsible for the production of the head of a boiling histotripsy
5 lesion. In [9, 30], we hypothesised that:

6 (a) a cavitation cluster formed between the HIFU transducer and a boiling vapour bubble is
7 likely to be due to the constructive interaction of a shockwave scattered by a bubble with the
8 incoming incident shockwaves;

9 (b) the magnitude of the backscattered acoustic pressure field may determine the formation of
10 and the site of bubble clouds during boiling histotripsy exposure.

11 To support our hypothesis, in this study, a numerical simulation of a 1.0 MHz HIFU field in
12 the presence of a bubble at its focus was carried out. The k-Wave MATLAB toolbox was used,
13 which numerically solves a system of first-order coupled equations (equivalent to the
14 generalised Westervelt equation). A qualitative analysis was conducted to understand basic
15 features of the interactions of a nonlinear wave with a bubble during boiling histotripsy
16 exposure. k-Wave has been previously used in a number of studies to simulate nonlinear wave
17 propagation through multiple tissue layers such as skin, muscle, strong scatterer such as ribs,
18 kidney and blood vessels [31, 32]. It is, however, worth noting that it has neither been
19 experimentally validated for fully capturing a strongly distorted nonlinear wave in
20 heterogeneous media, nor for propagation through high contrast materials. A very large number
21 of PPW and small CFL number are essentially necessary in order to model these, which
22 substantially increase memory requirements and computational time.

23

24 A number of studies have investigated the interaction between a shockwave and a single bubble
25 both numerically and experimentally in the field of extracorporeal shockwave lithotripsy

1 (ESWL) [38-42]. ESWL is the most common treatment for breaking down kidney stones.
2 Though P_+ and P_- used in boiling histotripsy are comparable to those in the shockwaves used
3 in ESWL, a lithotripter pulse which consists of a single cycle shock wave at the focus is
4 typically delivered at rates of 0.5 to 2 Hz [40], whereas a boiling histotripsy pulse with tens of
5 thousands of shockwave cycles at the HIFU focus is fired at around 1 Hz to induce mechanical
6 tissue damage. Therefore, most ESWL studies performed have focused on the investigation of
7 the impact of a single shock wave pulse of very high pressure amplitude (30 to 100 MPa) on a
8 bubble (e.g., changes of bubble wall motions). In contrast, in the present study, we have
9 extensively investigated, for the first time, the interference of incoming incident shockwaves
10 with backscattered acoustic fields by a bubble in order to understand the subsequent formation
11 of cavitation clouds in boiling histotripsy

12

13 ***4.1. Interaction of an incident shockwave with a bubble***

14 Canney et al [1] experimentally observed acoustic emissions from a shock wave heating-
15 induced boiling bubble in a tissue phantom, using an optical camera and a passive cavitation
16 detection (PCD) system. When a millimetre-sized boiling bubble formed at the HIFU focus, a
17 significant increase in the PCD voltage together with a sudden occurrence of higher order
18 multiple harmonic components of the fundamental frequency in the spectrogram was observed.
19 The authors speculated that these sudden changes, along with the formation of a boiling bubble,
20 were likely to be due to the reflection of the incident shockwaves from the bubble. This
21 reflection is due to the large acoustic impedance mismatch at the interface of the external
22 medium and the gas and water vapour bubble, according to the authors. The numerical results
23 depicted in Figures 7 to 9 clearly show the presence of scattering of the incident shock waves
24 by the vapour bubble. In addition, the constructive and destructive interactions of the scattered
25 field by the bubble with the incoming incident shock waves were also observed. This results in

1 the generation of localised peak negative pressures in the form of a layered structure separated
2 by about 0.8 mm (about half of the wavelength at 1 MHz). The peak negative pressure
3 magnitude between the acoustic fields simulated with and without the presence of a bubble at
4 the HIFU focus were compared. Interestingly, the peak negative pressure magnitude of the
5 backscattered field $P_{-, \text{backscatter}}$ appeared to be higher than that in the absence of a bubble at the
6 HIFU focus P_- (Figures 6b and 7b). For instance, P_- is -9.8 MPa whilst $P_{-, \text{backscatter}}$ is -31.36
7 MPa (a 3.2-fold increase, see Figure 8c-ii). The increase in the peak negative pressure
8 magnitude must therefore be attributable to the interaction of the acoustic field scattered by the
9 bubble with incoming incident shockwaves. This interference has been experimentally
10 examined in [33] where it was observed that bubble clouds began to form after a shockwave
11 impinged on a bubble in a gel phantom. The authors speculated that the reflection and inversion
12 of the peak positive pressure from the surface of the bubble interacted with the incoming
13 incident rarefactional phase, producing a greater peak negative pressure field than in the
14 absence of the bubble. This is known as the shock scattering effect [33] which is the main
15 mechanism of cavitation cloud histotripsy where a dense cavitation cluster induced by this
16 shock scattering effect mechanically destructs soft tissue. This shock scattering effect was also
17 observed in our numerical results shown in Figures 7c to e, Figures 8a-iii, b-iii, c-iii and Figures
18 9a-iii, b-iii, c-iii, d-iii. The shock scattering effect increases with the size of a bubble (Figure
19 8), the relative distance between the HIFU focus and a bubble (Figure 10) and the magnitude
20 of the peak positive phase of an incident shockwave (Figure 9 and Table 2).

21

22 ***4.2. Mechanisms of the formation of cavitation clouds in boiling histotripsy***

23 Maxwell et al [34] and Lin et al [35] reported that the cavitation cloud's intrinsic threshold is
24 around -28 MPa for most soft tissues. This is the lowest rarefaction pressure at which a dense
25 bubble cloud is almost certain to appear. In the present study, it was observed that the peak

1 negative pressure amplitude of the backscattered waves by a bubble gradually increased from
2 -17.4 MPa to -31.6 MPa as the bubble size increased (Figure 8c), which is above the pressure
3 threshold for cavitation clouds. These numerical results can explain our previous high speed
4 camera experimental observations of bubble dynamics during boiling histotripsy [9, 11, 30],
5 where a cavitation cluster did not appear immediately after the formation of a boiling vapour
6 bubble at the HIFU focus, but was rather observed when boiling bubble size increased beyond
7 a certain value (e.g. $480\ \mu\text{m}$).

8
9 Our numerical results suggest that cavitation clouds can migrate in the direction of the HIFU
10 transducer (i.e. the direction opposite to wave propagation) during the course of boiling
11 histotripsy exposure because of the shock scattering effect (Figure 7b). The reduction of
12 pressure amplitudes of backscattered fields due to tissue attenuation (Figure 7b and Figures 8a-
13 ii, b-ii and c-ii) would, however, limit this axial bubble cloud's growth. For instance, bubble
14 clouds would stop progressing when a backscattered acoustic pressure is below the cavitation
15 cloud's intrinsic threshold [9].

16

17 ***4.3. Prediction of the size of a lesion produced by boiling histotripsy***

18 The prediction of the shape and size of a boiling histotripsy lesion in soft tissue under a given
19 HIFU exposure condition would be of much interest to pre-treatment planning. The numerical
20 results presented in this study (Figures 7 to 9) together with [9, 11, 30] suggest that the
21 dimensions of the tail and the head of a boiling histotripsy lesion are dependent on the extent
22 of a localised shockwave heated region and the pressure magnitude of a backscattered acoustic
23 field by a boiling bubble, respectively.

24

1 To predict the size of a boiling histotripsy lesion, a numerical model capable of dealing with
2 scattering by localised heterogeneities is essentially required for simulating acoustic and
3 temperature fields in the presence of a bubble in soft tissue. This is mainly because a bubble
4 highly reflects and scatters an incident ultrasonic field (Figures 7 and 8), whereby the heat
5 deposition around a bubble is to be altered. For acoustic simulations, the full wave Westervelt
6 equation can possibly be employed to obtain the spatial distribution of nonlinear acoustic fields
7 around a vapour bubble in soft tissue. The bio-heat transfer equation, which accounts for the
8 effects of heat diffusion, blood perfusion and heat deposition [36], could then subsequently be
9 used in order to simulate the spatio-temporal distribution of the temperature field. These
10 aforementioned numerical approaches could predict the changes in the extent of a heated region
11 where a boiling vapour bubble is likely to form as a function of time. Along with this, bubble
12 dynamics simulations as developed and performed in [11, 13] may also be useful for predicting
13 how much tissue volume can potentially be destroyed within the heated zone.

14

15 Lastly, the size of the head of a boiling histotripsy lesion could possibly be predicted by
16 generating a contour plot of a simulated backscattered field by a boiling bubble where the
17 contour lines are equal to or above the cavitation cloud's intrinsic threshold. This contour plot
18 would indicate the potential site where cavitation clouds are likely to be induced. It has been
19 demonstrated that acoustic pressure is the main component which triggers bubble nucleation
20 in boiling histotripsy. However, HIFU heat deposition can also facilitate nucleation by reducing
21 nucleation pressure thresholds [10]. In boiling histotripsy, shock wave heating increases tissue
22 temperature, thereby decreasing the pressure threshold for cavitation clouds with time.
23 Vlaisavljevich et al [37] have shown that the cavitation cloud's intrinsic threshold reduces from
24 -29.8 MPa at 10°C to -14.9 MPa at 90°C . This temperature- and pressure- dependent cavitation
25 threshold should therefore be accounted for. For instance, modified classical nucleation theory

1 developed in [10], which predicts preferential bubble nucleation sites at a given acoustic
2 pressure and temperature during HIFU exposure, could be employed. Future work will be
3 focused on the prediction of the overall size of a tadpole shaped lesion resulting from a given
4 boiling histotripsy exposure condition.

5

6 **5. Conclusions**

7 In this work, the interactions of a shock wave with a vapour bubble during boiling histotripsy
8 were numerically investigated. To the best of our knowledge, this is the first study reporting
9 the mechanism underpinning the formation of cavitation clouds in boiling histotripsy. Our
10 results clearly demonstrate the interference of a scattered shockwave by a bubble with an
11 incoming incident shockwave, particularly in the rarefactional phase. This can induce a greater
12 peak negative pressure field compared to that in the absence of a bubble at the HIFU focus. In
13 addition, the backscattered pressure amplitude gradually increases with increasing bubble size,
14 and it can go beyond the intrinsic cavitation threshold of -28 MPa. These results reveal that
15 the shock scattering effect is likely to be the principle mechanism responsible for the
16 subsequent formation of cavitation clouds after the production of a primary boiling vapour
17 bubble at the HIFU focus during the course of boiling histotripsy. Our numerical results suggest
18 that the formation of cavitation clouds in boiling histotripsy is a threshold effect which
19 primarily depends on the size and location of a boiling bubble and the sum of the incident and
20 scattered pressure from a bubble.

21

22 **Acknowledgements**

23 This work was supported by the National Research Council of Science & Technology (NST)
24 grant by the Korea government (MSIT) (No. CAP-18-01-KIST) and Department of Mechanical

1 Engineering, University College London, UK.

2

3 **References**

4

5 [1] M.S. Canney, V.A. Khokhlova, O.V. Bessonova, M.R. Bailey, L.A. Crum, Shock-induced
6 heating and millisecond boiling in gels and tissue due to high intensity focused ultrasound,
7 *Ultrasound Med. Biol.* 36 (2010) 250–267.

8

9 [2] T.D. Khokhlova, M.S. Canney, V.A. Khokhlova, O.A. Sapozhnikov, L.A. Crum, M.R.
10 Bailey, Controlled tissue emulsification produced by high intensity focused ultrasound shock
11 waves and millisecond boiling, *J. Acoust. Soc. Am.* 130 (2011) 3498–3510.

12

13 [3] V.A. Khokhlova, J.B. Fowlkes, W.W. Roberts, G.R. Schade, Z. Xu, T.D. Khokhlova, T.L.
14 Hall, A.D. Maxwell, Y.N. Wang, C.A. Cain, Histotripsy methods in mechanical disintegration
15 of tissue: towards clinical applications, *Int. J. Hyperthermia* 31 (2015) 145–162.

16

17 [4] Y.N. Wang, T. Khokhlova, M. Bailey, J.H. Hwang, V. Khokhlova, Histological and
18 biochemical analysis of mechanical and thermal bioeffects in boiling histotripsy lesions
19 induced by high intensity focused ultrasound, *Ultrasound in Med. Biol.* 39(2013) 424–438.

20

21 [5] T.D. Khokhlova, Y.N. Wang, J.C. Simon, B.W. Cunitz, F. Starr, M. Paun, L.A. Crum, M.R.
22 Bailey, V.A. Khokhlova, Ultrasound-guided tissue fractionation by high intensity focused
23 ultrasound in an in vivo porcine liver model, *Proc. Natl. Acad. Sci. U.S.A.* 111 (2014) 8161–
24 8166.

25

26 [6] K.J. Pahk, G.H. Mohammad, M. Malago, N. Saffari, D.K. Dhar, A novel approach to
27 ultrasound-mediated tissue decellularization and intra-hepatic cell delivery in rats, *Ultrasound*
28 *Med. Biol.* 42 (2016) 1958–1967.

29

30 [7] A. Eranki, N. Farr, A Partanen, K.V. Sharma, H. Chen, C.T. Rossi, S.V.V.N. Kothapalli, M.
31 Oetgen, A. Kim, A.H. Negussie, D. Woods, B.J. Wood, P.C.W. Kim, P.S. Yarmolenko,
32 Boiling histotripsy lesion characterization on a clinical magnetic resonance imaging-guided
33 high intensity focused ultrasound system, *PLoS One.* 12 (2017) e0173867.

34

35 [8] T.D. Khokhlova, J.H. Hwang, HIFU for palliative treatment of pancreatic cancer, *J.*
36 *Gastrointest. Oncol.* 2 (2011) 175–184.

37

38 [9] K.J. Pahk, P. Gélât, D. Sinden, D.K. Dhar, N. Saffari, Numerical and experimental study
39 of mechanisms involved in boiling histotripsy, *Ultrasound Med. Biol.* 43 (2017) 2848–2861.

40

41 [10] M.O. de Andrade, S.R. Haqshenas, K.J. Pahk, N. Saffari, The effects of ultrasound
42 pressure and temperature fields in millisecond bubble nucleation, *Ultrason. Sonochem.* 55
43 (2019) 262 – 272.

44

45 [11] K.J. Pahk, M.O. de Andrade, P. Gélât, H. Kim, N. Saffari N, Mechanical damage induced
46 by the appearance of rectified bubble growth in a viscoelastic medium during boiling
47 histotripsy exposure, *Ultrason. Sonochem.* 53 (2019) 164–177.

- 1 [12] W. Kreider, M.R. Bailey, O.A. Sapozhnikov, V.A. Khokhlova, L.A. Crum, The dynamics
2 of histotripsy bubbles, 9-12 June 2010, Tokyo, Japan. 1359, AIP Conf. Proc. 10th Int. Symp.
3 on Therapeutic Ultrasound (ISTU 2010), 2011, pp. 427–430.
4
- 5 [13] K.J. Pahk, P. G elat, H. Kim, N. Saffari, Bubble dynamics in boiling histotripsy, *Ultrasound*
6 *Med. Biol.* 44 (2018) 2673–2696.
7
- 8 [14] B.E. Treeby, B.T. Cox, k-Wave: MATLAB toolbox for the simulation and reconstruction
9 of photoacoustic wave fields, *J. Biomed. Opt.* 15 (2010) 1–12.
10
- 11 [15] G. Taraldsen, A generalized Westervelt equation for nonlinear medical ultrasound, *J.*
12 *Acoust. Soc. Am.* 109 (2001) 1329–1333.
13
- 14 [16] B. Treeby, B. Cox, J. Jaros, K-Wave User Manual 1.1: A MATLAB toolbox for the time
15 domain simulation of acoustic wave fields (2016). Available at [http://www.k-](http://www.k-wave.org/manual/k-wave_user_manual_1.1.pdf)
16 [wave.org/manual/k-wave_user_manual_1.1.pdf](http://www.k-wave.org/manual/k-wave_user_manual_1.1.pdf).
17
- 18 [17] K. Wang, E. Teoh, J. Jaros, B.E. Treeby, Modelling nonlinear ultrasound propagation in
19 absorbing media using the k-Wave toolbox: experimental validation, *IEEE Int. Ultrason.*
20 *Symp.*, 7-10 October, 2012, Dresden, Germany, pp. 523–526.
21
- 22 [18] E. Martin, B.E. Treeby, Experimental validation of computational models for large-scale
23 nonlinear ultrasound simulations in heterogeneous, absorbing fluid media, *AIP Conf. Proc.*
24 *Recent Developments in Nonlinear Acoustics*, 29 June-3 July 2015,  cully, France. 1685,
25 p.070007.
26
- 27 [19] E. Martin, J. Jaros, B. Treeby, Experimental validation of k-Wave: nonlinear wave
28 propagation in layered, absorbing fluid media, *IEEE Transactions on Ultrasonics,*
29 *Ferroelectrics, and Frequency Control.* 67 (2019) 81–91.
30
- 31 [20] B.E. Treeby, J. Jaros, A.P. Rendell, B.T. Cox, Modeling nonlinear ultrasound propagation
32 in heterogenous media with power law absorption using a k-space pseudospectral method, *J.*
33 *Acoust. Soc. Am.* 131 (2012) 4324–4336.
34
- 35 [21] M. Tabei, T.D. Mast, R.C. Waag. A k-space method for coupled first-order acoustic
36 propagation equations, *J. Acoust. Soc. Am.* 111 (2002) 53–63.
37
- 38 [22] R.O. Cleveland, J.A. McAteer, The physics of shock wave lithotripsy, In: in Smith, A.D.
39 ed. *Smith’s Textbook on Endourology*. Hamilton: Decker (2007), 317–332.
40
- 41 [23] L. Crum, M. Bailey, J. H. Hwang, V. Khokhlova, O. Sapozhnikov, Therapeutic ultrasound:
42 recent trends and future perspectives, *Physics Procedia.* 3 (2010) 25–34.
43
- 44 [24] M.J. Choi, S.R. Guntur, K.I. Lee, D.G. Paeng, A. Coleman, A tissue mimicking
45 polyacrylamide hydrogel phantom for visualizing thermal lesions generated by high intensity
46 focused ultrasound, *Ultrasound Med. Biol.* 39 (2013) 439–448.
47

- 1 [25] Engineering ToolBox, (2008). Gases - Speed of Sound. [online] Available at:
2 https://www.engineeringtoolbox.com/speed-sound-gases-d_1160.html [Accessed 09. Jan.
3 2019].
4
- 5 [26] M.J. Moran, H.N. Shapiro, Fundamentals of Engineering Thermodynamics, 7th edition
6 (2015). Table A-2.
7
- 8 [27] L. Kakevicius, A. Demcenko, Ultrasound attenuation dependence on air temperature in
9 closed chambers, *Ultragarsas*. 63 (2008) 18–22.
10
- 11 [28] R.T. Beyer, The parameter B/A, [in:] *Nonlinear Acoustic*, M.F. Hamilton, D. T.
12 Blackstock [Eds.], Academic Press, New York. (1998) 25–39.
13
- 14 [29] J.S. Mendousse. Nonlinear dissipative distortion of progressive sound waves at moderate
15 amplitudes, *J. Acoust. Soc. Am.* 25(1953) 51–54.
16
- 17 [30] K.J. Pahk, M.O. de Andrade, H. Kim, N. Saffari, The effects of the size of a boiling bubble
18 on lesion production in boiling histotripsy, *Journal of Physics Conference Series* 1184 (2019b)
19 012007.
20
- 21 [31] N. Barnat, A. Grisey, B. Lecuelle, J. Anquez, B. Gerold, S. Yon, J.F. Aubry, Noninvasive
22 vascular occlusion with HIFU for venous insufficiency treatment: preclinical feasibility
23 experience in rabbits, *Physics in Medicine* 64 (2019) 025003.
24
- 25 [32] V. Suomi, J. Jaros, B. Treeby, R.O. Cleveland, Full modelling of high-intensity focused
26 ultrasound and thermal heating in the kidney using realistic patient models, *IEEE Transactions*
27 *on Biomedical Engineering* 65(2019). 969–979.
28
- 29 [33] A.D. Maxwell, T.Y. Wang, C.A. Cain, J.B. Fowlkes, O.A. Sapozhnikov, M.R. Bailey, Z.
30 Xu, Cavitation clouds created by shock scattering from bubbles during histotripsy, *J. Acoust.*
31 *Soc. Am.* 130 (2011) 1888–1898.
32
- 33 [34] A.D. Maxwell, C.A. Cain, T.L. Hall, J.B. Fowlkes, Z. Xu, Probability of cavitation for
34 single ultrasound pulses applied to tissues and tissue mimicking materials, *Ultrasound Med*
35 *Biol.* 39 (2013) 449–465.
36
- 37 [35] K.W. Lin, Y. Kim, A. Maxwell, T.Y. Wang, T.L. Hall, Z. Xu, J.B. Fowlkes, C.A. Cain,
38 *Histotripsy beyond the intrinsic cavitation threshold using very short ultrasound pulses:*
39 *microtripsy*, *IEEE Trans. Ultrason. Ferroelectr. Freq. Control* 61 (2014) 251–265.
40
- 41 [36] H.H. Pennes, Analysis of tissue and arterial blood temperatures in the resting human
42 forearm, *Journal of Applied Physiology* 1 (1948) 93–122.
43
- 44 [37] E. Vlaisavljevich, Z. Xu, A. D. Maxwell, L. Mancina, X. Zhang, K. Lin, A. P. Duryea, J.
45 R. Sukovich, T. L. Hall, E. Johnsen, C. A. Cain, Effects of temperature on the histotripsy
46 intrinsic threshold for cavitation, *IEEE Trans. Ultrason. Ferroelectr. Freq. Control* 63 (2016)
47 1064 – 1077.
48

1 [38] Z. Ding, S.M. Gracewski, The behaviour of a gas cavity impacted by a weak or strong
2 shock wave, *J. Fluid Mech.* 309 (1996) 183–209.

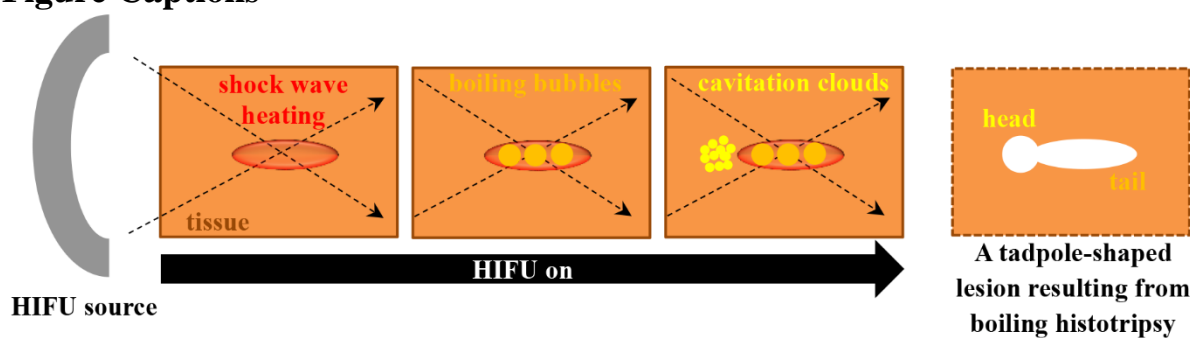
3
4 [39] E. Klaseboer, S.W. Fong, C.K. Turangan, B.C. Khoo, A.J. Szeri, M.L. Calvisi, G.N.
5 Sankin, P. Zhong, Interaction of lithotripter shockwaves with single inertial cavitation bubbles,
6 *J. Fluid Mech.* 593 (2007) 33–56.

7
8 [40] E. Johnsen, T. Colonius, Shock-induced collapse of a gas bubble in shockwave lithotripsy,
9 *J. Acoust. Soc. Am.* 124 (2008) 2011–2020.

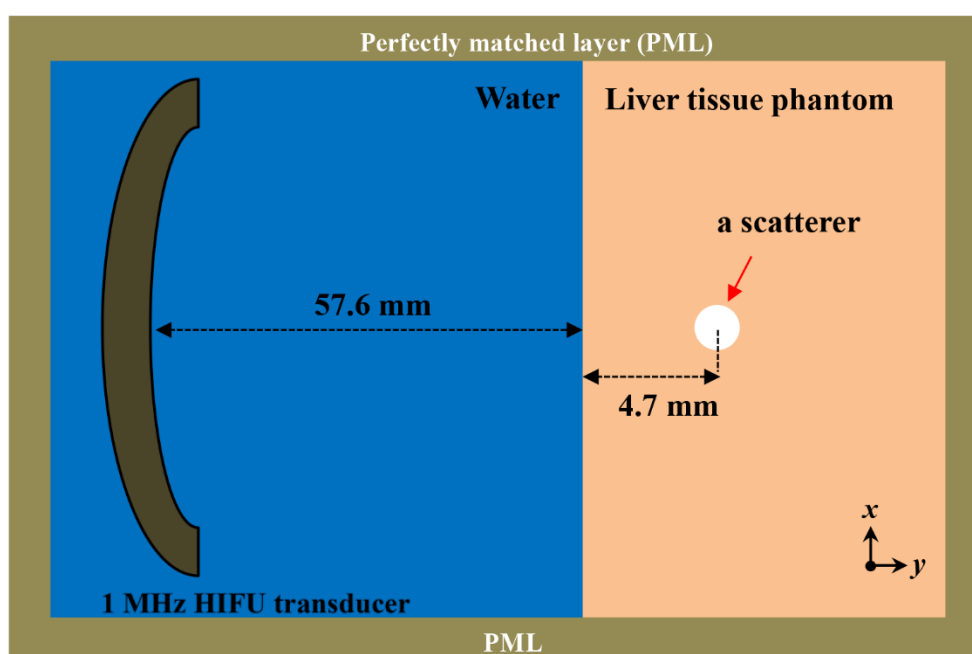
10
11 [41] N.A. Hawker, Y. Ventikos, Interaction of a strong shockwave with a gas bubble in a liquid
12 medium: a numerical study, *J. Fluid Mech.* 701 (2012) 59–97.

13
14 [42] R. Oguri, K. Ando, Cavitation bubble nucleation induced by shock-bubble interaction in
15 a gelatin gel, *Phys. Fluid* 30 (2018) 051904.

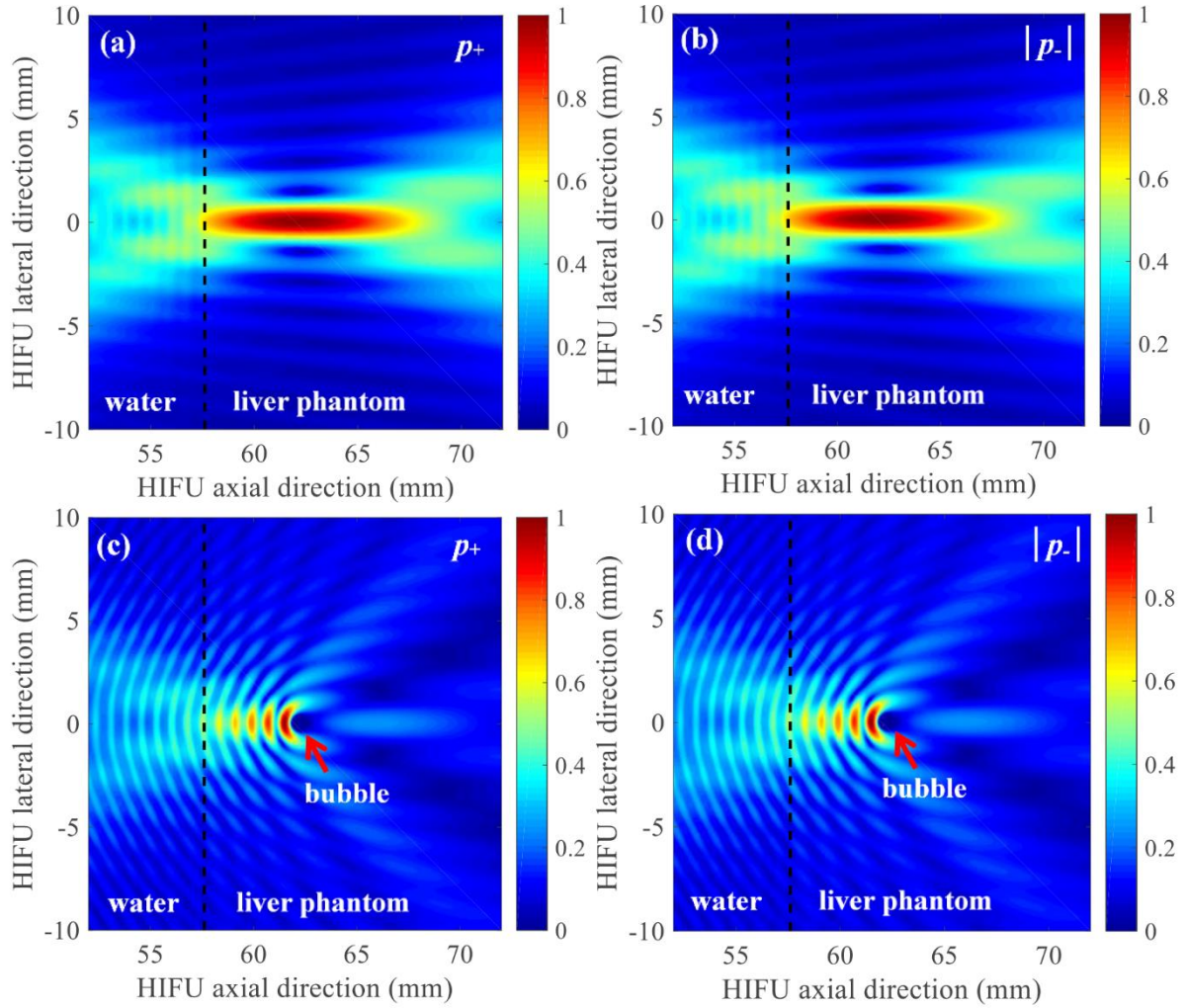
16
17
18
19
20
21
22
23
24
25
26
27
28
29
30
31
32
33
34
35
36
37
38
39
40
41
42
43
44

1 **Figure Captions**

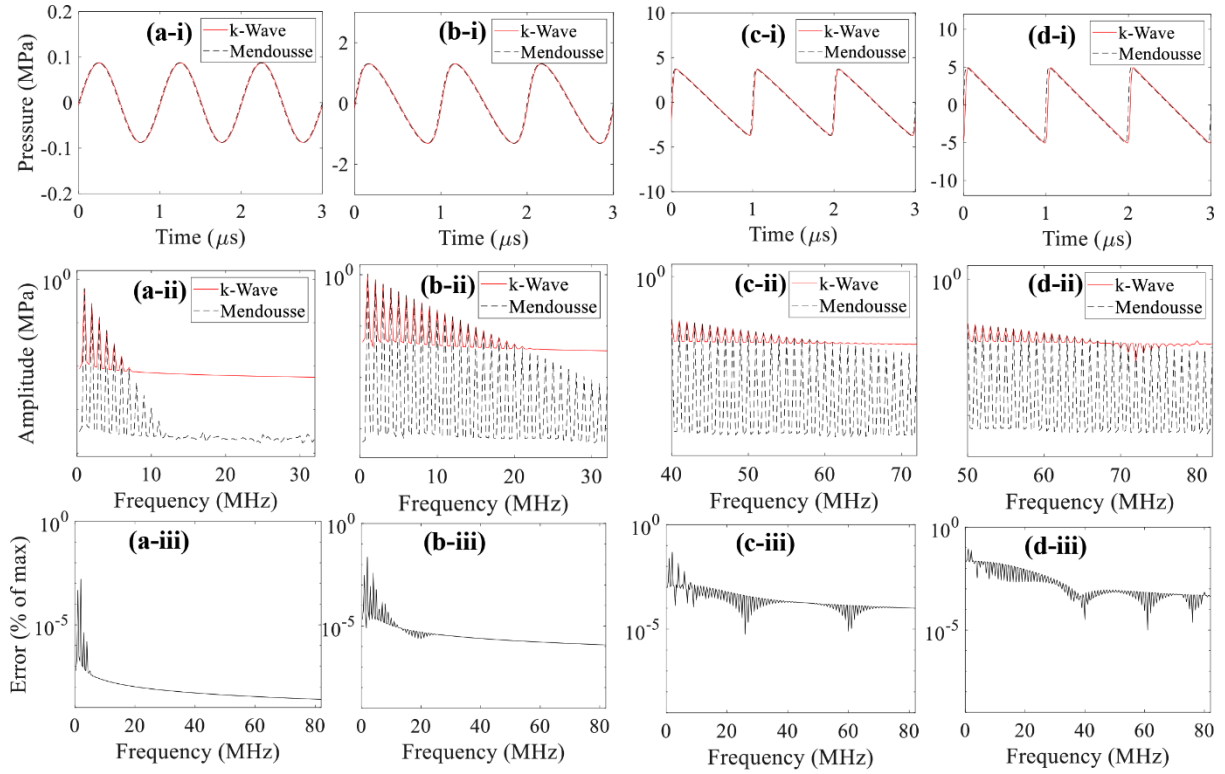
2
3 **Figure 1.** A schematic diagram illustrating the production of a tadpole-shaped lesion due to
4 the formation of boiling bubbles and cavitation clouds in boiling histotripsy.
5



6
7 **Figure 2.** A geometrical 2D model used in the simulation performed in the present study (figure
8 not to scale).
9

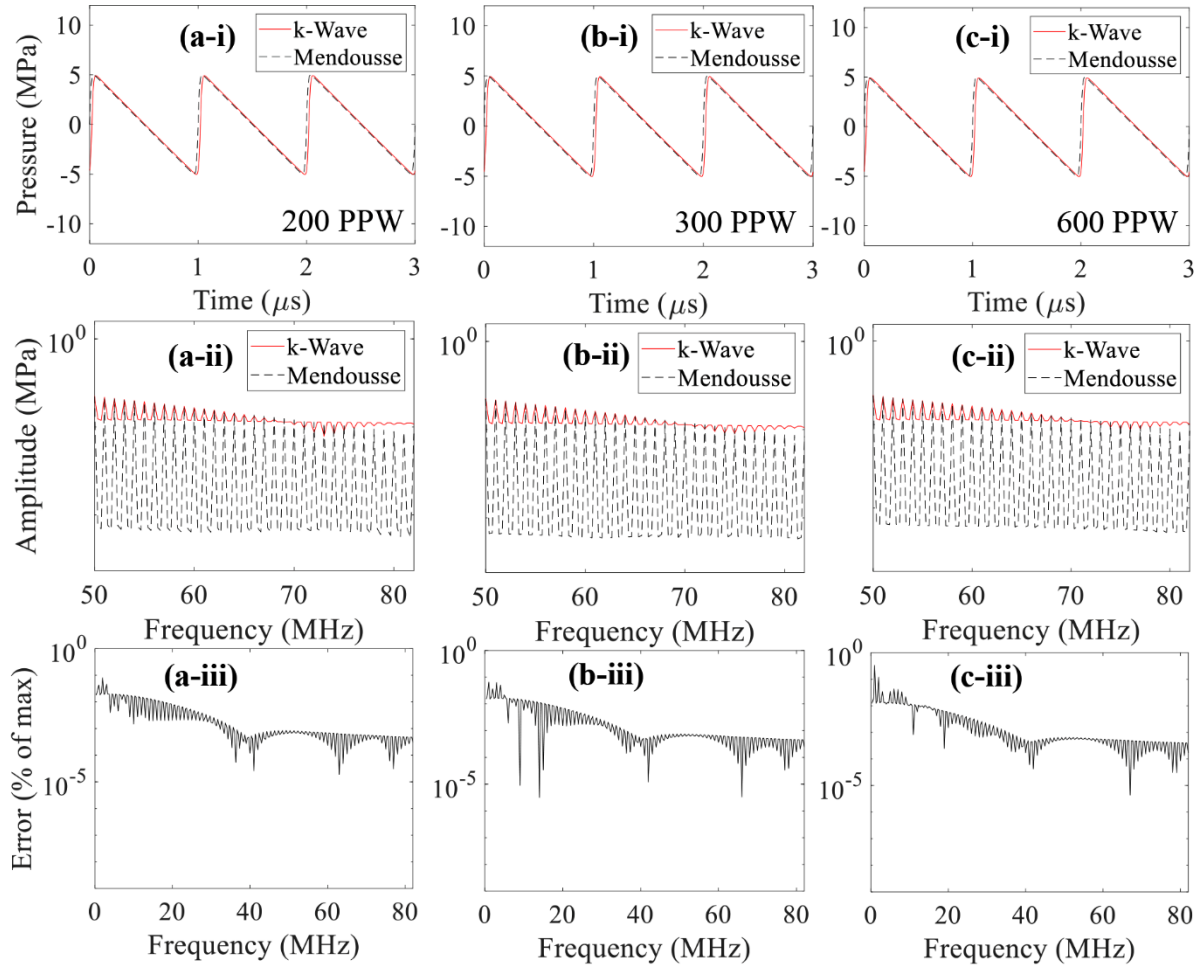


1
 2 **Figure 3.** Normalised simulated 2D spatial distribution of acoustic pressure fields without (a,
 3 b) and with (c, d) the presence of a bubble at the HIFU focus under linear propagation
 4 conditions. (a) and (c) are the simulated positive pressure fields p_+ whereas (b) and (d) are the
 5 magnitude of the computed negative pressure fields $|p_-|$. A bubble with a radius of $386 \mu\text{m}$ is
 6 indicated by an arrow in (c) and (d). The 1.0 MHz HIFU beam propagates from left to right.
 7 The simulations were performed over $t = 60 \mu\text{s}$. A bubble was modelled as a stationary 2D
 8 infinite cylinder.

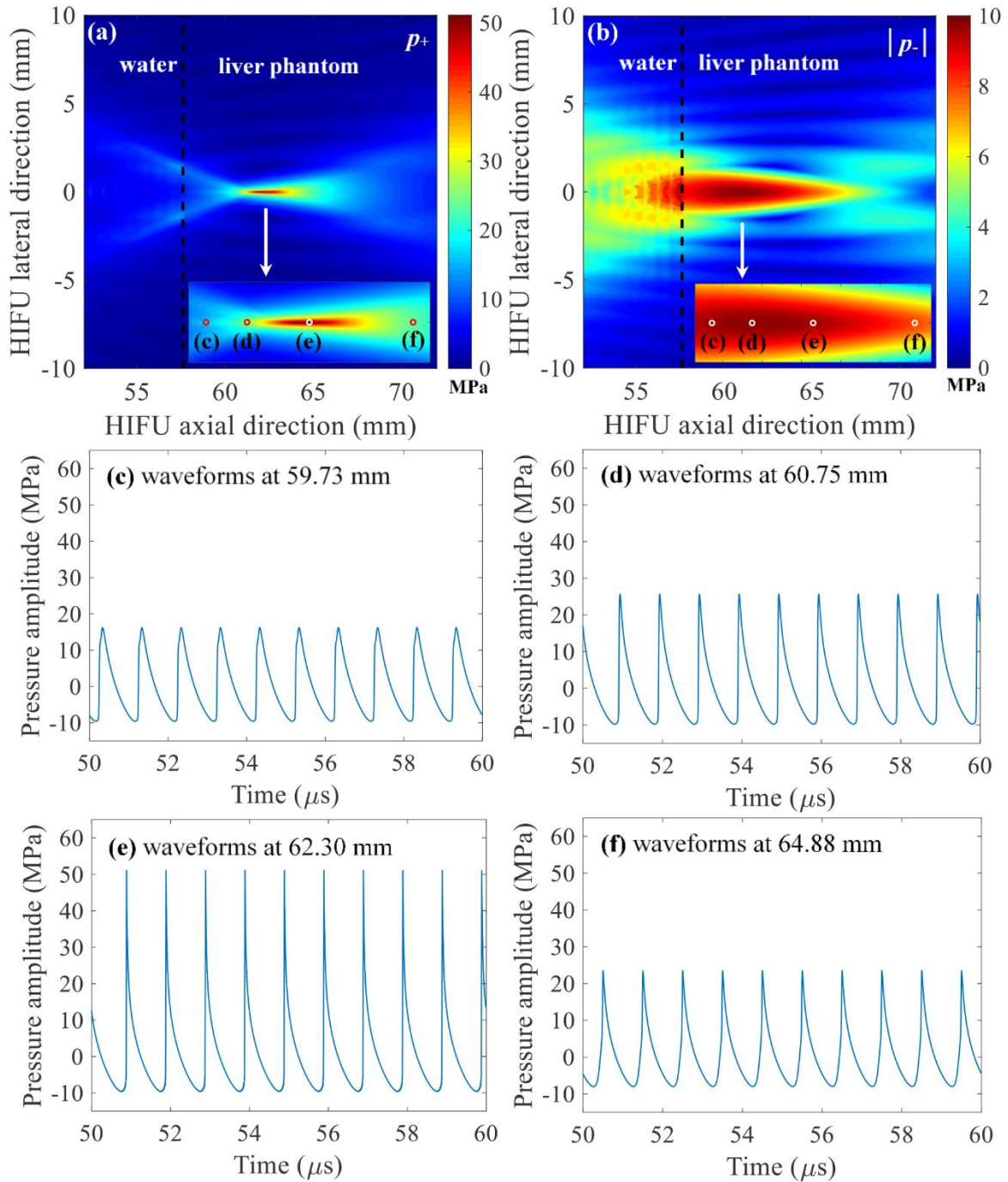


1
2
3
4
5
6
7
8

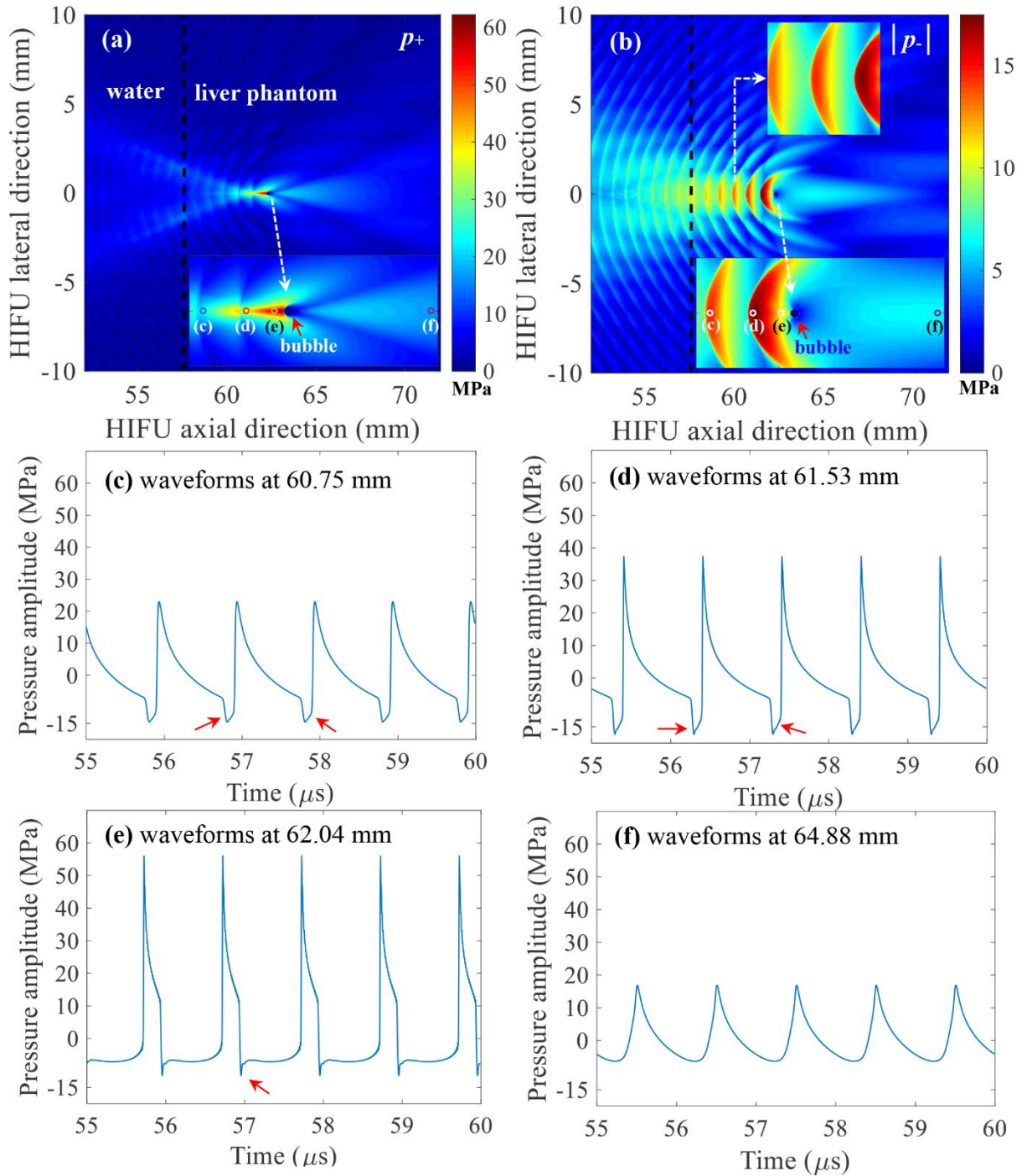
Figure 4. 1D convergence test results of the propagation of plane progressive waves in the liver tissue phantom. Images a-i, b-i, c-i and d-i show the numerical (k-Wave, red solid line) and theoretical (Mendousse, black dashed line) results of the wave signal in time domain with an input source pressure of 0.1 MPa, 1.5 MPa, 5.0 MPa and 15 MPa, respectively. Corresponding continuous frequency spectra (a-ii, b-ii, c-ii, d-ii) and error as a percentage of the maximum amplitude (a-iii, b-iii, c-iii, d-iii) are depicted in the second and the last rows. 160 PPW and a CFL number of 0.05 were used.



1
2 **Figure 5.** 1D convergence test results of the generation of harmonics with (a) 200, (b) 300 and
3 (c) 600 PPW. Figures in the first row show the time domain wave signals (a-i, b-i, c-i) whereas
4 images in the second and the third rows represent corresponding continuous frequency spectra
5 (a-ii, b-ii, c-ii) and error as a percentage of the maximum amplitude (a-iii, b-iii, c-iii),
6 respectively. An input source pressure of 15 MPa and a CFL number of 0.05 were used. The
7 maximum supported frequencies in k-Wave are 100, 150 and 300 MHz at 200, 300 and 600
8 PPW.

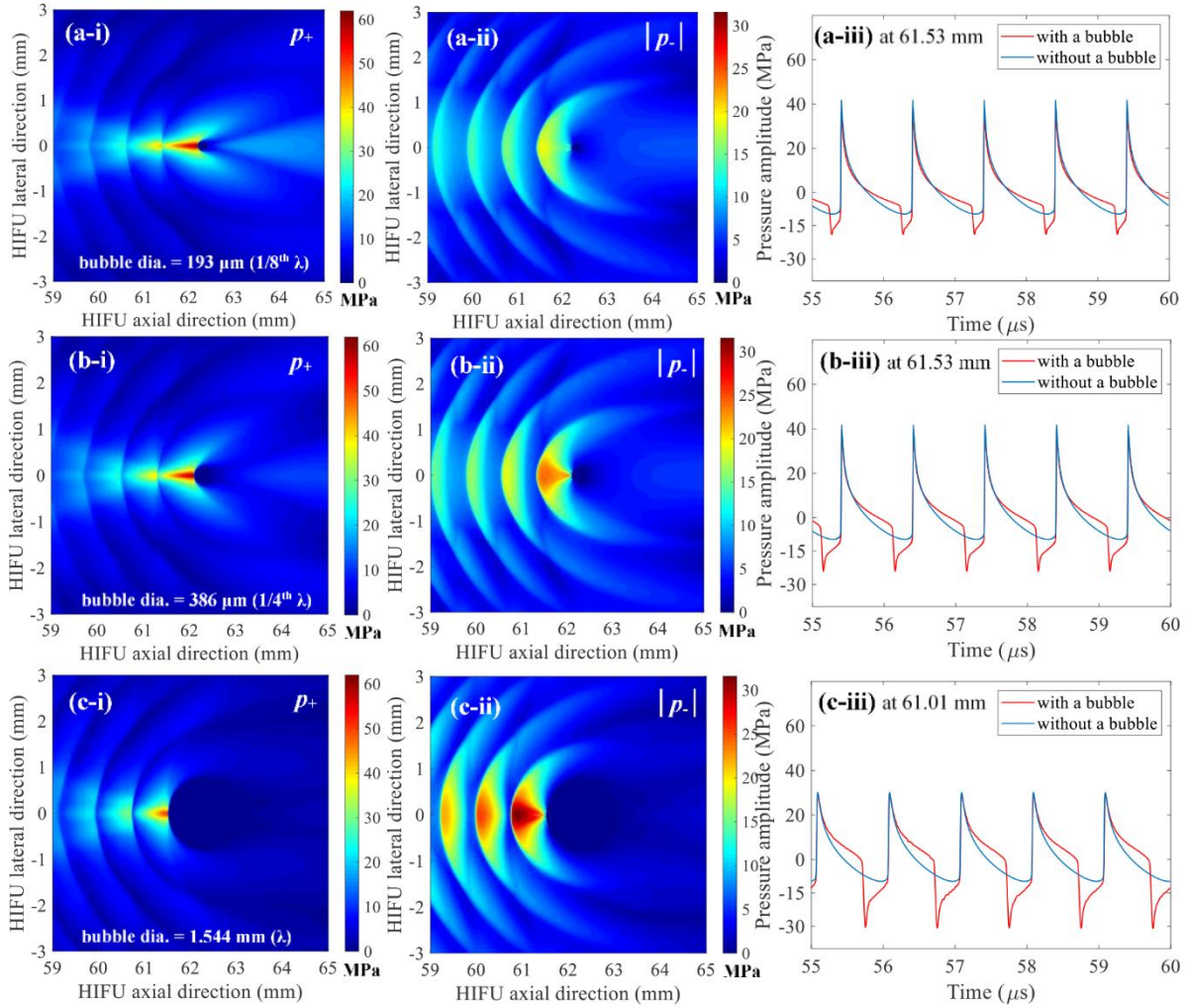


1
2 **Figure 6.** Simulated acoustic pressure fields in the absence of a vapour bubble at the HIFU
3 focus under nonlinear propagation conditions. (a) and (b) are the simulated 2D spatial
4 distributions of positive p_+ and negative $|p_-|$ pressure fields. Images (c) to (f) respectively
5 represent the waveforms at 59.73, 60.75, 62.30 and 64.88 mm in the HIFU axial direction. The
6 1.0 MHz HIFU beam with P_+ of 51.2 MPa and P_- of -9.8 MPa propagates from left to right.
7 The simulations were performed over $t = 60 \mu s$.



1
2 **Figure 7.** Simulated acoustic pressure fields in the presence of a vapour bubble at the HIFU
3 focus. (a) and (b) are the simulated 2D spatial distributions of positive p_+ and negative $|p_-|$
4 pressure fields. Images (c) to (f) respectively represent the waveforms at 60.75, 61.53, 62.04
5 and 64.88 mm in the HIFU axial direction. The presence of the constructive interference of the
6 backscattered shockwaves by the bubble with the incoming incident shockwaves is indicated
7 by the red arrows in (c), (d) and (e). The 1.0 MHz HIFU beam with P_+ of 51.2 MPa and P_- of
8 -9.8 MPa propagates from left to right. The diameter of the bubble used in the simulations
9 was $154 \mu\text{m}$ ($1/10^{\text{th}} \lambda$). The simulations were performed over $t = 60 \mu\text{s}$.

10
11
12



1
 2 **Figure 8.** The effects of the size of a bubble on the pressure amplitude of the backscattered
 3 acoustic fields. Images in the left column (a-i, b-i, c-i) represent the 2D spatial distribution of
 4 positive pressure fields p_+ whereas those in the middle column (a-ii, b-ii, c-ii) indicate 2D
 5 negative pressure fields $|p_-|$. Figures in the right column (a-iii, b-iii, c-iii) depict 1D
 6 waveforms with (red lines) or without (blue lines) a bubble at a given position in the HIFU
 7 axial direction (61.53 and 61.01 mm). The bubble size was varied as (a) 193 ($1/8^{\text{th}}$ of the
 8 wavelength), (b) 386 ($1/4^{\text{th}}$ of the wavelength) and (c) 1544 μm (equals to the wavelength). In
 9 the simulations, the bubble was exposed to 1.0 MHz nonlinear shocked waves with peak
 10 positive and negative pressures of $P_+ = 51.2$ MPa and $P_- = -9.8$ MPa at the HIFU focus. The
 11 simulations were performed over $t = 60$ μs . The HIFU beam propagates from left to right.

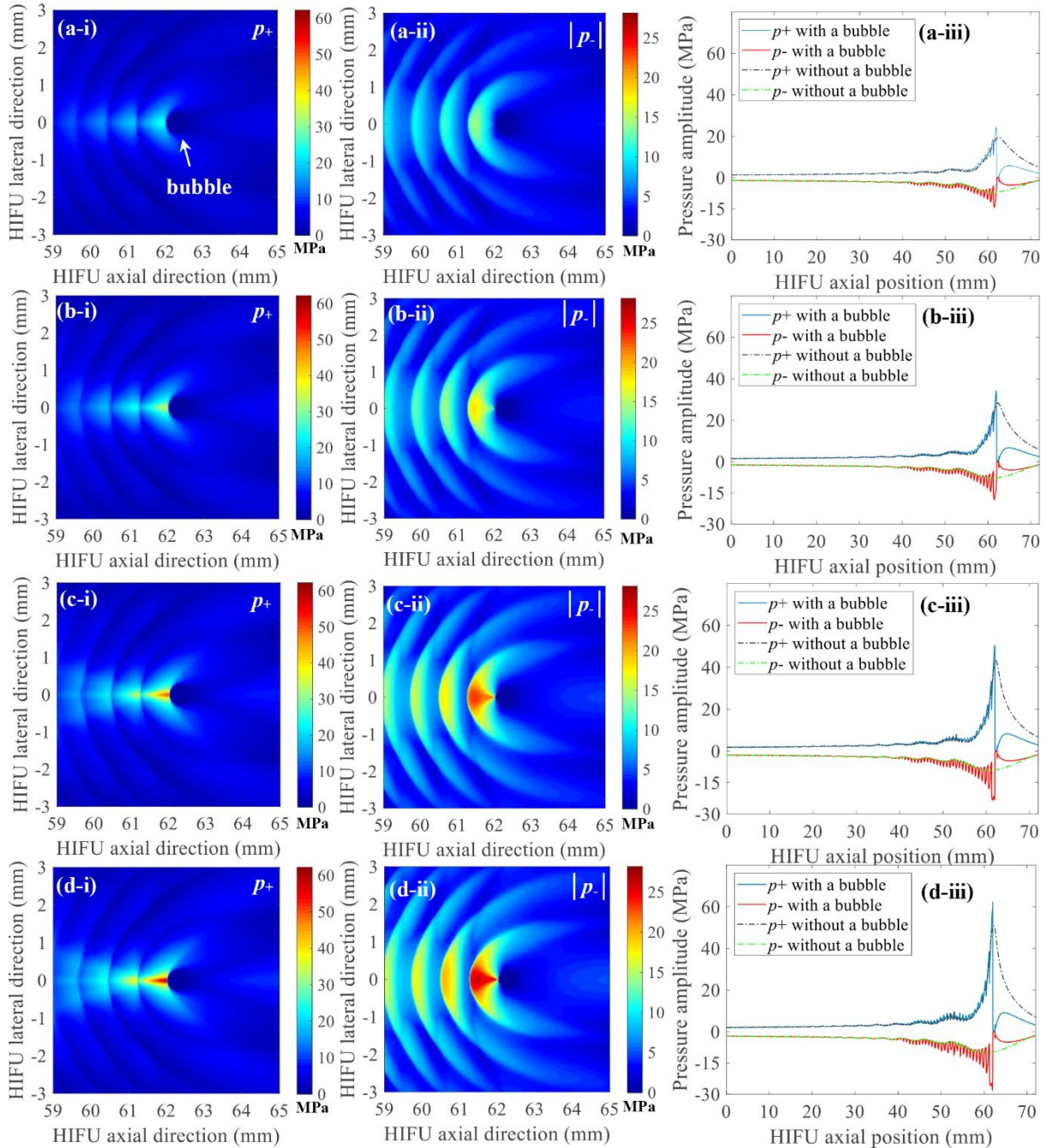
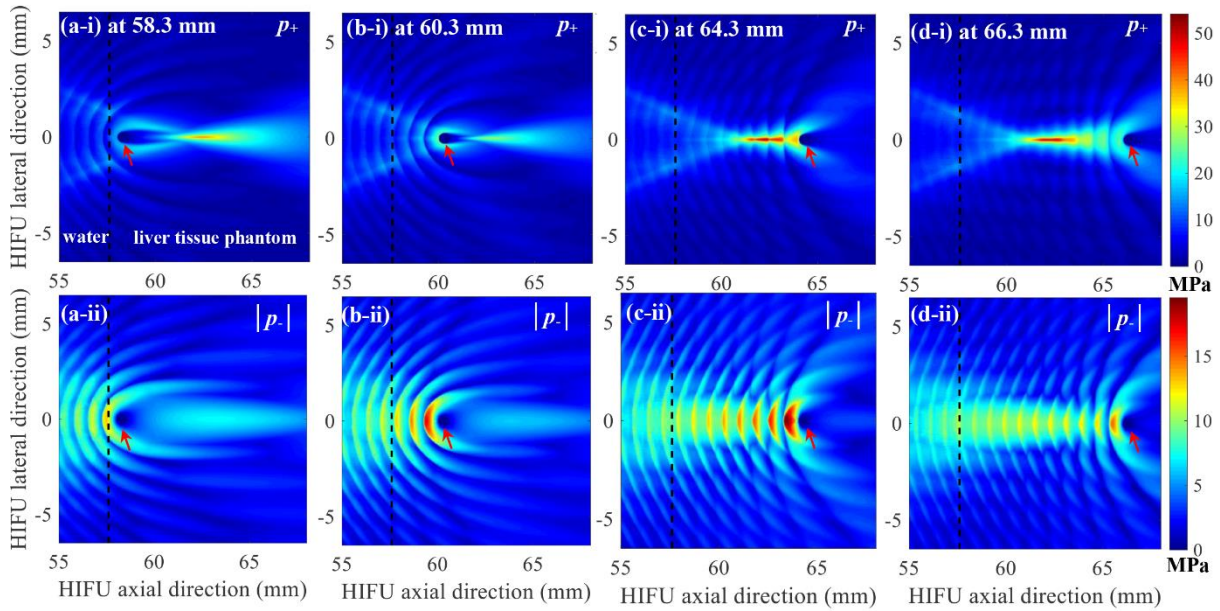


Figure 9. The effects of the changes in the pressure amplitudes of incident shockwaves ($P_{+, \text{incident}}$, $P_{-, \text{incident}}$) on backscattered acoustic fields by a bubble. Exposure conditions are as follows: (a) $P_{+, \text{incident}} = 19.5$ MPa; $P_{-, \text{incident}} = -6.9$ MPa. (b) $P_{+, \text{incident}} = 28.3$ MPa; $P_{-, \text{incident}} = -7.8$ MPa. (c) $P_{+, \text{incident}} = 43.3$ MPa; $P_{-, \text{incident}} = -9.0$ MPa. (d) $P_{+, \text{incident}} = 51.2$ MPa; $P_{-, \text{incident}} = -9.8$ MPa. Images in the left column (a-i, b-i, c-i, d-i) represent the 2D spatial distribution of positive pressure fields p_+ whereas those in the middle column (a-ii, b-ii, c-ii, d-ii) indicate 2D negative pressure fields $|p_-|$. Figures in the right column (a-iii, b-iii, c-iii, d-iii) depict the simulated 1D HIFU beam profile along the axis with or without the presence of a bubble at the HIFU focus. The bubble size used in the simulation was $515 \mu\text{m}$ ($1/3^{\text{rd}}$ of the wavelength). The simulations were performed over $t = 60 \mu\text{s}$. The HIFU beam propagates from left to right.

1
2
3
4
5
6
7
8
9
10
11
12



1
 2 **Figure 10.** The effects of the changes in the location of a bubble on backscattered acoustic
 3 fields in boiling histotripsy. Images on the first row (a, b, c and d-i) respectively represent the
 4 computed 2D spatial distributions of positive pressure fields p_+ with the presence of a bubble
 5 at 58.3, 60.3, 64.3 and 66.3 mm along the HIFU axial axis. The corresponding simulated 2D
 6 spatial distributions of negative pressure fields $|p_-|$ are shown in the second row (a, b, c and d-
 7 ii). In the simulations, the size of a bubble was kept constant ($515 \mu\text{m}$). The 1.0 MHz HIFU
 8 beam with P_+ of 51.2 MPa and P_- of -9.8 MPa propagates from left to right. The red arrows
 9 indicate the bubble.

10
 11
 12

13

14

15

16

17

18

19

20

21

22

1 Tables

2 **Table 1.** Physical properties used in the simulations.

3

	Water [17]	Liver tissue phantom [2, 24]	Water vapour bubble	Units
Speed of sound	1482	1544	477.5 [25]	m s ⁻¹
Density	1000	1044	0.598 [26]	kg m ⁻³
Attenuation coefficient	0.217	15	164* [27]	dB m ⁻¹ MHz ^{-y}
Nonlinear parameter (B/A)	5	6	0.4* [28]	-
Power law exponent (y)	2	0.93	2 [#]	-

4 *obtained for air. #assumed to equal to water.

5
6
7 **Table 2.** The effects of the changes in the pressure amplitudes of incident shockwaves on the
8 peak negative pressure magnitude of the backscattered acoustic fields by a bubble with a
9 diameter of 515 μm ($1/3^{\text{rd}}$ of the wavelength at 1 MHz).

10

Peak pressures of the incident wave* [MPa]		Peak negative pressure amplitude of the backscattered acoustic field $P_{-, \text{backscatter}}$ [MPa]
$P_{+, \text{incident}}$	$P_{-, \text{incident}}$	
19.5	- 6.9	- 14.28
28.3	- 7.8	- 18.17
43.3	- 9.0	- 23.32
51.2	- 9.8	- 28.17

11 *values simulated in the absence of a bubble.

12